J|A|C|S
ARTICLES

Published on Web 08/10/2009

Self-Association and Electron Transfer in Donor−Acceptor Dyads Connected by *meta*-Substituted Oligomers

Agustín Molina-Ontoria,[†] Gustavo Fernández,[†] Mateusz Wielopolski,[‡,§] Carmen Atienza,[‡] Luis Sánchez,[†] Andreas Gouloumis,[†] Timothy Clark,[§] Nazario Martín,*[,†,||] and Dirk M. Guldi*[,‡]

Departamento de Química Orgánica, Facultad de Química, Universidad Complutense, E-28040 Madrid, Department of Chemistry and Pharmacy and Interdisciplinary Center for Molecular Materials (ICMM), Friedrich-Alexander-Universität Erlangen-Nürnberg, Egerlandstrasse 3, 91058 Erlangen, Germany, Computer-Chemie-Centrum and ICMM, Department of Chemistry and Pharmacy, Friedrich-Alexander-Universität Erlangen-Nürnberg, Nägelsbachstrasse 25, 91052 Erlangen, Germany, and IMDEA-Nanociencia, E-28049 Madrid, Spain

Received March 26, 2009; E-mail: nazmar@quim.ucm.es; dirk.guldi@chemie.uni-erlangen.de

Abstract: The synthesis of a new series of electron donor−acceptor conjugates (**5**, **10**, **13**, and **16**) in which the electron acceptor—C_{60}—and the electron donor—π-extended tetrathiafulvalene (exTTF)—are bridged by means of *m*-phenyleneethynylene spacers of variable length is reported. The unexpected self-association of these hybrids was first detected to occur in the gas phase by means of MALDI-TOF spectrometry and subsequently corroborated in solution by utilizing concentration-dependent and variable-temperature ^{1}H NMR experiments. Furthermore, the ability of these new conjugates to form wirelike structures upon deposition onto a mica surface has been demonstrated by AFM spectroscopy. In light of their photoactivity and redoxactivity, **5**, **10**, **13**, and **16** were probed in concentration-dependent photophysical experiments. Importantly, absorption and fluorescence revealed subtle dissimilarities for the association constants, that is, a dependence on the length of the *m*-phenylene spacers. The binding strength is in **5** greatly reduced when compared with those in **10**, **13**, and **16**. Not only that, the spacer length also plays a decisive role in governing excited-state interactions in the corresponding electron donor−acceptor conjugates (**5**, **10**, **13**, and **16**). To this end, **5**, in which the photo- and electroactive constituents are bridged by just one aromatic ring, displays—exclusively and independent of the concentration (10^{-6} to 10^{-4} M)—efficient intramolecular electron transfer events on the basis of a "through-bond" mechanism. On the contrary, the lack of conjugation throughout the bridges in **10** (two *m*-phenyleneethynylene rings), **13** (three *m*-phenyleneethynylene rings), and **16** (four *m*-phenyleneethynylene rings) favors at low concentration (10^{-6} M) "through space" intramolecular electron transfer events. These are, however, quite ineffective and, in turn, lead to excited-state deactivations that are at high concentrations (10^{-4} M) dominated by intracomplex electron transfer events, namely, between exTTF of one molecule and C_{60} of another molecule, and that stabilize the resulting radical ion pair state with lifetimes reaching 4.0 μs.

Introduction

The implementation of flexible optoelectronic devices[1] and more specifically organic photovoltaics[2] requires the development of molecules able to perform important functions such as the absorption of light and its conversion into power. For this purpose, an efficient transport of electrons and holes through an organized network of p-type—usually soluble *p*-phenylenevinylene (PPV) or polythiophene (PT) polymer derivatives—and n-type—the most successful being the well-known fullerene derivative PCBM—components is required.[2] Prior to the mobility of the charge carriers, charge separation between the donor and acceptor moieties at the donor−acceptor interface is needed. This charge transfer event usually takes place between noncovalently linked species. A number of supramolecular model systems have been studied to demonstrate the effectiveness in which charge transfer can proceed.[3] Thus, supramolecular

[†] Universidad Complutense.
[‡] Department of Chemistry and Pharmacy and ICMM, Friedrich-Alexander-Universität Erlangen-Nürnberg.
[§] Computer-Chemie-Centrum and ICMM, Department of Chemistry and Pharmacy, Friedrich-Alexander-Universität Erlangen-Nürnberg.
[||] IMDEA-Nanociencia.

(1) (a) Special Issue on Organic Electronics. *Chem. Mater.* **2004**, *16*, 4381−4846. (b) Wassel, R. A.; Gorman, C. B. *Angew. Chem., Int. Ed.* **2004**, *43*, 5120–5123. (c) Carroll, R. L.; Gorman, C. B. *Angew. Chem., Int. Ed.* **2002**, *41*, 4378–4400. (d) Tour, J. M. *Acc. Chem. Res.* **2000**, *33*, 791–804.

(2) For recent reviews on PV cells, see: (a) Brabec, C. J.; Sariciftci, N. S.; Hummelen, J. C. *Adv. Funct. Mater.* **2001**, *11*, 15–26. (b) Coakley, K. M.; McGehee, M. D. *Chem. Mater.* **2004**, *16*, 4533–4542. (c) Günes, S.; Neugebauer, H. *Chem. Rev.* **2007**, *107*, 1324–1338. (d) Thompson, B. C.; Fréchet, J. M. J. *Angew. Chem., Int. Ed.* **2008**, *47*, 58–77.

(3) For reviews, see: (a) Wasielewski, M. R. *Chem. Rev.* **1992**, *92*, 435–461. (b) Sánchez, L.; Martín, N.; Guldi, D. M. *Angew. Chem., Int. Ed.* **2005**, *44*, 5374–5382. (c) D'Souza, F.; Ito, O. *Coord. Chem. Rev.* **2005**, *249*, 1410–1422. (d) Kawase, T.; Kurata, H. *Chem. Rev.* **2006**, *106*, 5250–5273. (e) Wasielewski, M. R. *J. Org. Chem.* **2006**, *71*, 5051–5066. (f) Pérez, E. M.; Martín, N. *Chem. Soc. Rev.* **2008**, *37*, 1512–1519.

 10.1021/ja9024269 CCC: $40.75

donor−acceptor assemblies connected by hydrogen-bonding arrays[3a,b] or coordinative metal bonds[3c,d] have been exploited in the quest for long-lived charge-separated states. However, detailed studies on charge transfer interactions in supramolecular assemblies held together by means of $\pi-\pi$ aromatic interactions are yet scarce, despite their implication in natural−charge transport through DNA bases[4a−c]—or artificial−charge transport in the active layer of photovoltaic devices[2,4d,e]—systems. An important requisite for these studies involves the connection of appropriate donor (D) and acceptor (A) moieties by bridges (B's) of different natures. Conjugates prepared by the combination of a variety of electron donor fragments, such as ferrocenes[5] or porphyrins,[6] and electron acceptor units, for instance, perylenebisimides,[7] have been utilized to investigate electron transfer processes in D−B−A conjugates upon light irradiation. In our research group, we have described a number of conjugates in which the electron donor is 2-[9-(1,3-dithiol-2-ylidene)anthracen-10(9*H*)-ylidene]-1,3-dithiole (exTTF)[8] and the electron acceptor unit is [60]fullerene,[9] connected by different covalent or supramolecular spacers.[10] Very recently, we have reported on the formation of supramolecular complexes from concave exTTF-based pincerlike receptors and the convex C_{60} surface in a positive homotropic cooperative manner.[11] These complexes experience an electron transfer through the $\pi-\pi$ stacking interactions that hold together some of these tweezers with C_{60} to form the corresponding supramolecular radical pair.[12]

In this paper we report on the synthesis and redox properties of a new family of D−B−A conjugates in which D is an exTTF fragment,[8] A is C_{60}, and the B groups are *m*-phenyleneethynylene oligomers of different lengths. We have chosen this class of spacer (i) because it is known that the promotion of an electron from the D to the A is favored in the excited state in only one way but not in the reverse one, that is, the charge recombination would be unfavored,[13] and (ii) because of the well-documented ability of *m*-phenyleneethynylenes to switch from random conformations in chlorinated solvents to helical arrangements in polar solvents due to the influence of solvophobic effects.[14] This situation allows us to study the competence between *inter*- or *intra*molecular electron transfer processes. Unexpectedly, these new hybrids self-associate by $\pi-\pi$ aromatic interactions to form aggregates as has been demonstrated by mass spectrometry, ^{1}H NMR experiments at different concentrations, and atomic force microscopy (AFM) imaging. Photophysical studies reveal the strong impact of the *meta* substitution on the photophysical properties for these new conjugates in comparison with our previous results reported for their *para*-conjugated congeners[15] as well as the concentration dependence of these properties as a consequence of the self-assembly process.

Results and Discussion

Synthesis. The synthesis of the final hybrids **5**, **10**, **13**, and **16** was carried out by stepwise approaches based on the preparation of asymmetrically functionalized π-conjugated oligo(*m*-phenyleneethynylene) (OMPE) spacers of different lengths endowed with a formyl group and exTTF at the terminal positions—compounds **4**, **9**, **12**, and **15** in Schemes 1 and 2. The preparation of the corresponding oligo(*m*-phenyleneethynylene) building blocks was performed by using Pd-catalyzed cross-coupling reactions between derivatized arylacetylenes and aryl halides.[16]

The synthesis of 3-ethynylbenzaldehyde (**2b**), an intermediate compound necessary for the preparation of dyad **5**, was carried out by using Sonogashira cross-coupling reaction (Pd/Cu

(4) (a) Elias, B.; Genereux, J. C.; Barton, J. K. *Angew. Chem., Int. Ed.* **2008**, *47*, 9067–9070. (b) Giese, B. *Bioorg. Med. Chem.* **2006**, *14*, 6139–6143. (c) Conwell, E. M. *Proc. Natl. Acad. Sci. U.S.A.* **2005**, *102*, 8795–8799. (d) Mynar, J. L.; Yamamoto, T.; Kosaka, A.; Fukushima, T.; Ishii, N.; Aida, T. *J. Am. Chem. Soc.* **2008**, *130*, 1530–1531. (e) Yamamoto, Y.; Fukushima, T.; Suna, Y.; Ishii, N.; Saeki, A.; Seki, S.; Tagawa, S.; Taniguchi, M.; Kawai, T.; Aida, T. *Science* **2006**, *314*, 1761–1764.

(5) (a) González-Rodríguez, D.; Torres, T.; Olmstead, M. M.; Rivera, J.; Herranz, M. A.; Echegoyen, L.; Atienza Castellanos, C.; Guldi, D. M. *J. Am. Chem. Soc.* **2006**, *128*, 10680–10681. (b) Jeon, W. S.; Moon, K.; Park, S. H.; Chun, H.; Ko, Y. H.; Lee, J. Y.; Lee, E. S.; Samal, S.; Selvapalam, N.; Rekharsky, M. V.; Sindelar, V.; Sobransingh, D.; Inoue, Y.; Kaifer, A. E.; Kim, K. *J. Am. Chem. Soc.* **2005**, *127*, 12984–12989.

(6) (a) D'Souza, F.; Chitta, R.; Sandanayaka, A. S. D.; Subbaiyan, N. K.; D'Souza, L.; Araki, Y.; Ito, O. *J. Am. Chem. Soc.* **2007**, *129*, 15865–15871. (b) Li, W.-S.; Kim, K. S.; Jiang, D.-L.; Tanaka, H.; Kawai, T.; Kwon, J. H.; Kim, D.; Aida, T. *J. Am. Chem. Soc.* **2006**, *128*, 10527–10532. (c) Imahori, H.; Sekiguchi, Y.; Kashiwagi, Y.; Sato, T.; Araki, Y.; Ito, O.; Yamada, H.; Fukuzumi, S. *Chem.—Eur. J.* **2004**, *10*, 3184–3196. (d) Jiang, D.-L.; Choi, C.-K.; Honda, K.; Li, W.-S.; Yuzawa, T.; Aida, T. *J. Am. Chem. Soc.* **2004**, *126*, 12084–12089.

(7) (a) Zhang, R.; Wang, Z.; Wu, Y.; Fu, H.; Yao, J. *Org. Lett.* **2008**, *10*, 3065–3068. (b) Beckers, E. H. A.; Meskers, S. C. J.; Schenning, A. P. H. J.; Chen, Z.; Würthner, F.; Marsal, P.; Beljonne, D.; Cornil, J.; Janssen, R. A. J. *J. Am. Chem. Soc.* **2006**, *128*, 649–657. (c) Marcos Ramos, A.; Meskers, S. C. J.; Beckers, E. H. A.; Prince, R. B.; Brunsveld, L.; Janssen, R. A. J. *J. Am. Chem. Soc.* **2004**, *126*, 9630–9644.

(8) (a) Yamashita, Y.; Kobayashi, Y.; Miyashi, T. *Angew. Chem., Int. Ed. Engl.* **1989**, *28*, 1052–1053. (b) Bryce, M. R.; Moore, A. J.; Hasan, M.; Ashwell, G. J.; Fraser, A. T.; Clegg, W.; Hursthouse, M. B.; Karaulov, A. I. *Angew. Chem., Int. Ed. Engl.* **1990**, *29*, 1450–1452. (c) Martín, N.; Sánchez, L.; Seoane, C.; Ortí, E.; Viruela, P. M. *J. Org. Chem.* **1998**, *63*, 1268–1279. (d) Segura, J. L.; Martín, N. *Angew. Chem., Int. Ed.* **2001**, *40*, 1372–1409.

(9) (a) Echegoyen, L.; Echegoyen, L. E. *Acc. Chem. Res.* **1998**, *31*, 593–601. (b) Guldi, D. M.; Prato, M. *Acc. Chem. Res.* **2000**, *33*, 695–703. (c) Guldi, D. M. *Chem. Commun.* **2000**, 321–327. (d) Martín, N. *Chem. Commun.* **2006**, 2093–2104.

(10) Martín, N.; Sánchez, L.; Herranz, M. A.; Illescas, B. M.; Guldi, D. M. *Acc. Chem. Res.* **2007**, *40*, 1015–1024.

(11) (a) Pérez, E. M.; Sánchez, L.; Fernández, G.; Martín, N. *J. Am. Chem. Soc.* **2006**, *128*, 7172–7173. (b) Pérez, E. M.; Sierra, M.; Sánchez, L.; Torres, M. R.; Viruela, R.; Viruela, P. M.; Ortí, E.; Martín, N. *Angew. Chem., Int. Ed.* **2007**, *46*, 1847–1851. (c) Fernández, G.; Pérez, E. M.; Sánchez, L.; Martín, N. *Angew Chem., Int. Ed.* **2008**, *47*, 1094–1097. (d) Fernández, G.; Pérez, E. M.; Sánchez, L.; Martín, N. *J. Am. Chem. Soc.* **2008**, *130*, 2410–2411. (e) Fernández, G.; Sánchez, L.; Pérez, E. M.; Martín, N. *J. Am. Chem. Soc.* **2008**, *130*, 10674–10683.

(12) Gayathri, S. S.; Wielopolski, M.; Pérez, E. M.; Fernández, G.; Sánchez, L.; Viruela, R.; Ortí, E.; Guldi, D. M.; Martín, N. *Angew. Chem., Int. Ed.* **2009**, *48*, 815–819.

(13) (a) Thompson, A. L.; Ahn, T.-S.; Thomas, K. R. J.; Thayumanavan, S.; Martinez, T. J.; Bardeen, C. J. *J. Am. Chem. Soc.* **2005**, *127*, 16348–16349. (b) Gaab, K. M.; Thompson, A. L.; Xu, J.; Martinez, T. J.; Bardeen, C. J. *J. Am. Chem. Soc.* **2003**, *125*, 9288–9289.

(14) (a) Nelson, J. C.; Saven, J. G.; Moore, J. S.; Wolynes, P. G. *Science* **1997**, *277*, 1793–1796. (b) Prince, R. B.; Saven, J. G.; Moore, J. S.; Wolynes, P. G. *J. Am. Chem. Soc.* **1999**, *121*, 3114–3121. (c) Lahiri, S.; Thompson, J. L.; Moore, J. S. *J. Am. Chem. Soc.* **2000**, *122*, 11315–11319.

(15) (a) Wielopolski, M.; Atienza, C.; Clark, T.; Guldi, D. M.; Martín, N. *Chem.—Eur. J.* **2008**, *14*, 6379–6390. (b) Figueira-Duarte, T. M.; Gégout, A.; Nierengarten, J. F. *Chem. Commun.* **2007**, 109–119. (c) Atienza, C.; Martín, N.; Wielopolski, M.; Haworth, N.; Clark, T.; Guldi, D. M. *Chem. Commun.* **2006**, 3202–3204.

(16) (a) Sonogashira, K. In *Comprehensive Organic Synthesis*; Trost, B. M., Fleming, I., Eds.; Pergamon Press: Oxford, U.K., 1991. (b) Sonogashira, K. In *Metal-Catalyzed Cross-Coupling Reactions*; Diederich, F., Stang, P. J., Eds.; Wiley-VCH: Weinheim, Germany, 1998. (c) Sonogashira, K. *J. Organomet. Chem.* **2002**, *653*, 46–49. (d) Eisler, S.; Chahal, N.; McDonald, R.; Tykwinski, R. R. *Chem.—Eur. J.* **2003**, *9*, 2542–2550. (e) Mohr, W.; Stahl, J.; Hampel, F.; Galysz, J. A. *Chem.—Eur. J.* **2003**, *9*, 3324–3340. (f) Eisler, S.; Slepkov, A. D.; Elliott, E.; Luu, T.; McDonald, R.; Hegmann, F. A.; Tykwinski, R. R. *J. Am. Chem. Soc.* **2005**, *127*, 2666–2676.

Scheme 1. Synthesis of **5**[a]

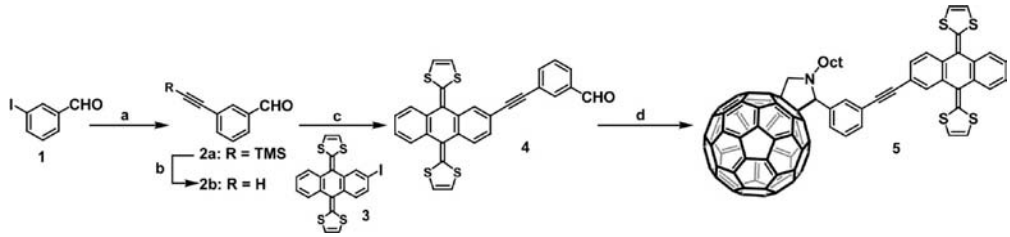

[a] Reagents and conditions: (a) $PdCl_2(PPh_3)_2$, CuI, THF, piperidine, TMSA, 83%; (b) K_2CO_3, 99%, THF/MeOH (1:1); (c) compound **3**, $PdCl_2(PPh_3)_2$, CuI, THF, piperidine, 47%; (d) C_{60}, *N*-octylglycine, PhCl, Δ, 40%.

Scheme 2. Synthesis of **10**, **13**, and **16**[a]

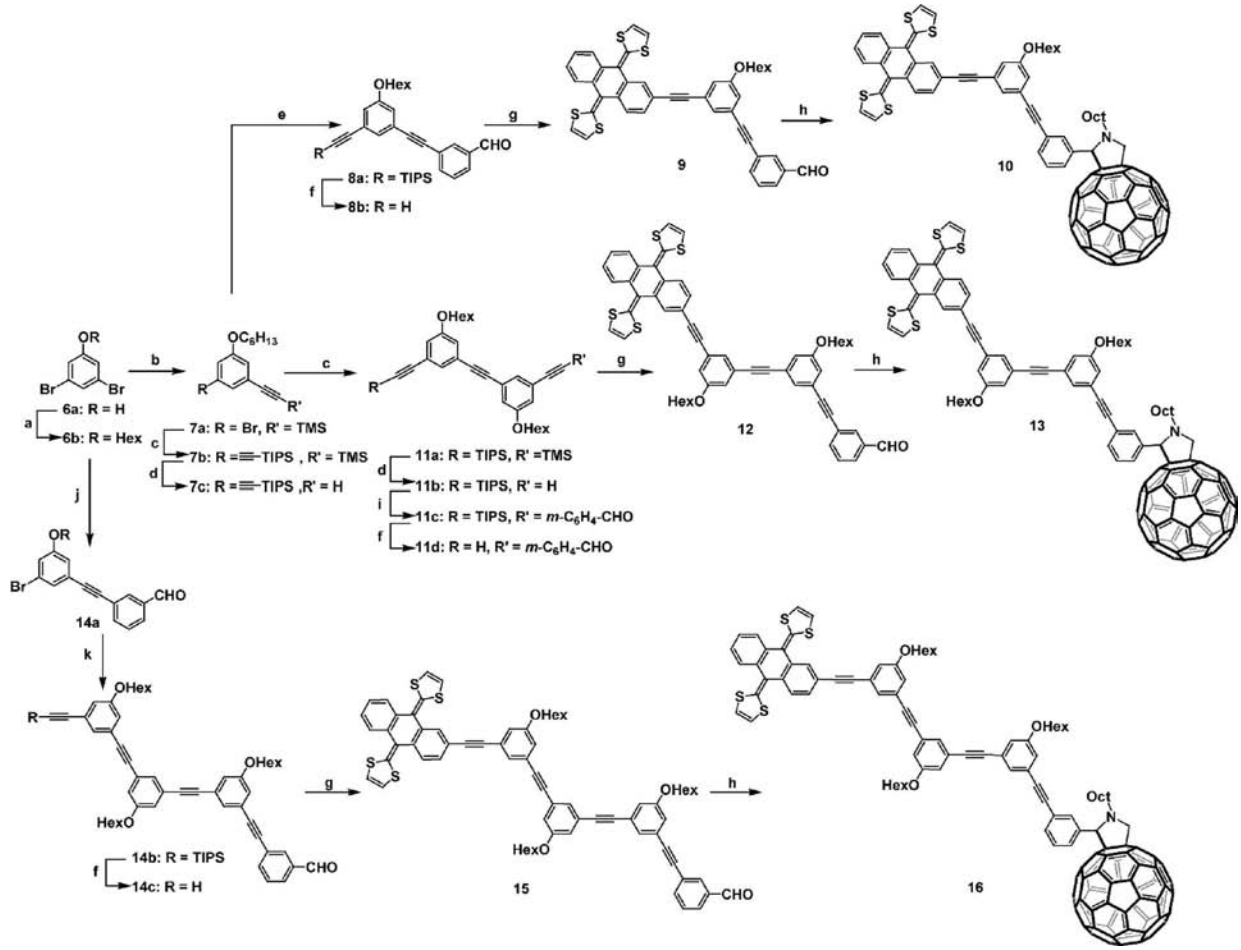

[a] Reagents and conditions: (a) K_2CO_3, 2-butanone, hexyl bromide, 99%; (b) $PdCl_2(PPh_3)_2$, CuI, THF, piperidine, TMSA, 80%; (c) $PdCl_2(PPh_3)_2$, CuI, THF, piperidine, TIPSA, 92%; (d) K_2CO_3, THF/MeOH; (e) $PdCl_2(PPh_3)_2$, CuI, THF, piperidine, compound **1**, 94%; (f) Bu_4NF, 72% (for **11d**), 69% (for **14c**); (g) $PdCl_2(PPh_3)_2$, CuI, THF, piperidine, compound **3**, 63% (for **4**), 57% (for **9**), 53% (for **12**), 69% (for **15**); (h) C_{60}, *N*-octylglycine, PhCl, Δ, 54% (for **10**), 63% (for **13**), 65% (for **16**); (i) $Pd_2(dba)_3$, $AsPh_3$, THF, Pr^i_2NH, compound **1**, 77%; (j) $PdCl_2(PPh_3)_2$, CuI, THF, piperidine, compound **2b**, 45%; (k) $Pd_2(dba)_3$, $AsPh_3$, THF, NEt_3, 47%.

catalytic system) between the commercially available 3-iodobenzaldehyde and (trimethylsilyl)acetylene (TMSA) in 82% overall yield, after trimethylsilyl group cleavage with potassium carbonate (Scheme 1).[17]

Aryldiacetylenes emerged as valuable precursors for a bidirectional stepwise synthesis of the spacers bearing two to four phenylethynyl groups (Scheme 2). For the stepwise synthesis of the unsymmetrically substituted aryldiacetylene **7b** we followed a literature procedure.[18] In particular, commercially available 3,5-dibromophenol (**6a**) led first through the formation of phenol ether **6b** and then through two sequential Sonogashira cross-coupling reactions between **6b**, TMSA, and (triisopropylsilyl)acetylene (TIPSA) to compounds **7a** and **7b**, respectively. Cleaving the TMS group with potassium carbonate—a procedure that ensures the integrity of the TIPS groups—is the key toward compound **7c**, which was obtained in quantitative yield. A Sonogashira cross-coupling reaction between com-

(17) Vidal-Ferran, A.; Müller, C. M.; Sanders, J. K. M. *J. Chem. Soc., Chem. Commun.* **1994**, 2657–2658.

(18) Grave, C.; Lentz, D.; Schafer, A.; Samorí, P.; Rabe, J. P.; Franke, P.; Schluter, A. D. *J. Am. Chem. Soc.* **2003**, *125*, 6907–6918.

pounds **2b** and **7c** leads to the unsymmetrically substituted compound **8a**, which after cleavage of the TIPS group with tetrabutylammonium fluoride (TBAF) affords **8b** in 73% yield.

Similarly, the preparation of bisaryldiacetylene **11a** was carried out by a Sonogashira cross-coupling reaction, but in this case between compounds **7a** and **7c**. Following cleavage of the TMS groups, compound **11b** was obtained in 98% yield. The reaction of the latter with compound **1** via a modified Sonogashira copper-free protocol using $Pd_2(dba)_3/AsPh_3$ as the catalytic system,[19] to avoid Glaser-type homocoupling reactions, led to compound **11c**. The final TIPS cleavage that yields **11d** was, however, performed with potassium fluoride, since TBAF started to degrade the formyl groups.

For the synthesis of compound **14c** a convergent synthetic protocol was applied. Essentially, using the Sonogashira protocol in the reaction between compounds **2b** and **6b**, compound **14a** is obtained in 45% yield. **14a** and **11b** were converted to **14b** via the modified Sonogashira copper-free catalytic system. Following the treatment with potassium fluoride to cleave the TIPS group, compound **14c** was isolated in 38%.

The syntheses of the precursors bearing the exTTF moieties (i.e., **4**, **9**, **12**, and **15**) are outlined in Schemes 1 and 2. We applied the same catalytic protocol—$Pd(PPh_3)_4$, CuI, and dry triethylamine at 60 °C for 5−7 h—in the cross-coupling reactions between compounds **2b**, **8b**, **11d**, and **14c** and **3**[20] to obtain these red solid intermediates with yields varying from 33% to 69%.

Finally, **5**, **10**, **13**, and **16** were obtained by 1,3-dipolar cycloaddition of the corresponding azomethine ylides, generated in situ from *N*-octylglycine and aldehydes **4**, **9**, **12**, and **15** with C_{60}.[21] **5**, **10**, **13**, and **16** were obtained as brown solids in yields ranging from 40% to 65%.

All compounds and intermediates were characterized by means of analytical and spectroscopic techniques. The FTIR spectra showed, for example, the characteristic peaks of the carbonyl group in the precursors **4**, **9**, **12**, and **15** at around 1700 cm^{-1}, while the peak at around 525 cm^{-1} confirms the presence of C_{60} in **5**, **10**, **13**, and **16**. The ^1H NMR and ^{13}C NMR spectra reveal the expected resonance signals of aliphatic and aromatic protons and carbons; see for details the Supporting Information. Typical signals are, for example, those that correspond to the pyrrolidine protons at $\delta \approx 5.1$, $\delta \approx 5.0$, and $\delta \approx 4.1$.

Redox Properties. The electrochemical properties of conjugates (**5**, **10**, **13**, and **16**) and their precursors (**4**, **9**, **12**, and **15**) have been investigated by cyclic voltammetry (CV) and differential pulse voltammetry (DPV) in a solvent mixture containing *o*-dichlorobenzene (oDCB)/acetonitrile (4:1); see Table 1 and Figure 2. Furthermore, pristine C_{60} and the TIPS-protected tetramer decorated with the aldehyde functionality (**14b**) have also been utilized as reference compounds.

Three quasi-reversible reduction processes refer in all C_{60}-based conjugates to the first, second, and third reduction of the fullerene moiety (Figure 1). Nevertheless, the saturation of a double bond in C_{60}, as a consequence of the functionalization, shifts the reduction cathodically relative to that of pristine C_{60}.

Table 1. Redox Potentials (V) of C_{60}−OMPE−exTTF Conjugates **5**, **10**, **13**, and **16** and Their Precursors

compd[a]	E^1_{red}	E^2_{red}	E^3_{red}	E^1_{oxid}	E^2_{oxid}
C_{60}	−0.843	−1.294	−1.758		
5	−0.901	−1.299	−1.841	+0.330	+1.792
10	−0.872	−1.260	−1.794	+0.230	+1.680
13	−0.869	−1.257	−1.799	+0.226	+1.626
16	−0.872	−1.250	−1.792	+0.282	+1.661
4	−1.794[b]			+0.296	+1.752
9	−1.984[b]			+0.203	+1.744
12	−2.028[b]			+0.216	+1.683
15	−2.036[b]			+0.257	+1.631
14b	−2.006[b]				+1.774

[a] Experimental conditions: V vs $Ag/AgNO_3$, oDCB/CH_3CN (4:1) as solvent, GCE as working electrode, Pt as counter electrode, Bu_4NClO_4 (0.1 M) as supporting electrolyte, scan rate 100 mV s^{-1}. The concentration of the sample in all the measurements was 0.3 mM. [b] Corresponding to the aldehyde functionality.

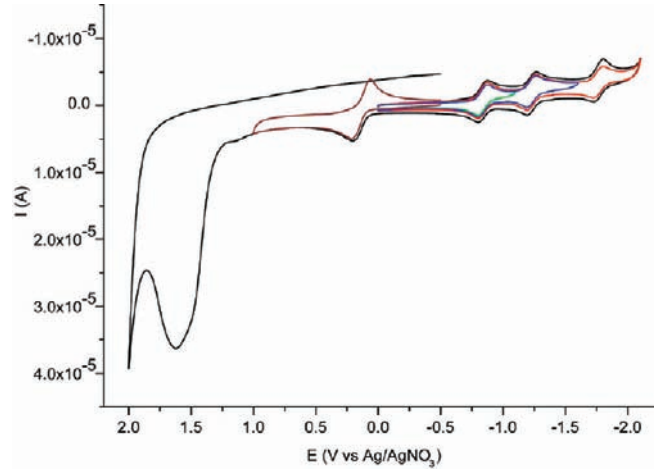

Figure 1. Cyclic voltammograms of **13** (∼0.3 mM) in *o*-dichlorobenzene/acetonitrile (4:1) utilizing 0.1 M Bu_4NClO_4 as the supporting electrolyte and a glassy carbon as the working electrode at a scan rate of 100 mV s^{-1}.

In none of the conjugates is the highly energetic process at ∼−2 V, which corresponds to reduction of the aldehyde group, discernible (Table 1). Regarding the anodic region of the voltammograms, all the conjugates show two oxidation waves at ∼+0.2 and ∼+1.7 V, respectively (Figure 1). The first quasireversible oxidation wave corresponds to the loss of two electrons by the exTTF moiety.[22] Only for the first congener of the series (i.e., **5**) is the oxidation shifted by about 0.2 V when compared to the rest of the series (i.e., **10**, **13**, and **16**). Implicit is a better electronic communication between C_{60} and exTTF.

The second oxidation process corresponds to that of the *meta*-conjugated bridges—a conclusion that stems from the analysis of **14b**.[23] In fact, only two waves are seen in the voltammogram of **14b**: One wave evolves around −2 V, a process that corresponds to the reduction of the aldehyde functionality, see also the reactivity of **4**, **9**, **12**, and **15**—and another wave appears at +1.7 V, which is ascribed to the oxidation of the bridge. In **5**, even the oxidation of the bridge is shifted anodically, when

(19) Wagner, R. W.; Johnson, T. E.; Li, F.; Lindsey, J. S. *J. Org. Chem.* **1995**, *60*, 5266–5273.
(20) Díaz, M. C.; Illescas, B. M.; Seoane, C.; Martín, N. *J. Org. Chem.* **2004**, *69*, 4492–4499.
(21) (a) Maggini, M.; Scorrano, G.; Prato, M. *J. Am. Chem. Soc.* **1993**, *115*, 9798–9799. (b) Tagmatarchis, N.; Prato, M. *Synlett* **2003**, 768–779.
(22) (a) Bryce, M. R.; Moore, A. J. *J. Chem. Soc., Perkin Trans. 1* **1991**, 157–168. (b) Bryce, M. R.; Moore, A. J. *J. Chem. Soc., Chem. Commun.* **1991**, *22*, 1638–1639. (c) Batsanov, A. S.; Bryce, M. R.; Coffin, M. A.; Green, A.; Hester, R. E.; Howard, J. A. K.; Lednev, I. K.; Martín, N.; Moore, A. J.; Moore, J. N.; Ortí, E.; Sánchez, L.; Savirón, M.; Viruela, P. M.; Viruela, R.; Ye, T. *Chem.—Eur. J.* **1998**, *4*, 2580–2592.

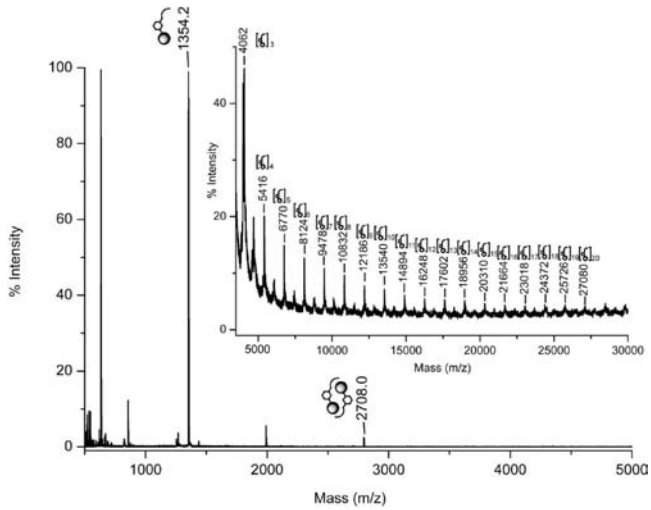

Figure 2. MALDI-TOF mass spectra of **5** in a ditranol matrix. The inset illustrates the formation of supramolecular oligomers (i.e., up to the 20-mer) in the gas phase.

compared to the remaining conjugates. It is most probable that a combined effect, namely, fewer number of rings together with a more efficient interaction with the acceptor, is responsible for this trend. In summary, our redox data—together with the information extracted from the electronic absorption spectra (see below)—suggest the existence of weak electronic communications between the electroactive units in the new conjugates in their ground states.

Self-Association. At first glance, the structural characterization of **5** as performed with MALDI-TOF mass spectrometry just confirmed the molecular mass with an *m*/*z* value of 1354. Nevertheless, a weaker peak is seen at $m/z = 2708$. Notable is the difference between these two *m*/*z* values, which leads us to hypothesize that a 2-mer of **5** is formed. A carefully performed analysis of the MALDI-TOF spectrum brings as many as 20 peaks—all spaced by the same molecular mass of 1354—to light (Figure 2). Consequently, we must assume the systematic aggregation of **5**, whose aggregate size ranges from the formation of the 2-mer all the way to the 20-mer. Such findings—including our previously reported C_{60}–exTTF hybrids[24]—indicate the unexpected ability of **5** to self-associate in the gas phase.[12,25]

Similar MALDI-TOF analyses have also been carried out for **10**, **13**, and **16**. Importantly, in all the cases aggregates are formed reflecting the spontaneous self-assembly of the monomeric units with molecular ions for **10** (i.e., $m/z = 1554$), **13** (i.e., $m/z = 1754$), and **16** (i.e., $m/z = 1954$). The number of self-assembled units of the corresponding conjugate is inversely proportional to the molecular mass of the conjugate. In addition to the aforementioned **5**, formation of up to the 14-mer is observed for **10**, whereas **13** and **16** tend to form up to the 11-mer and 6-mer, respectively (Figures S2–S4, Supporting Information).[26]

Evidence for the ability of systems **5**, **10**, **13**, and **16** to self-assemble in solution has been obtained by concentration-dependent ^{1}H NMR experiments carried out in $CDCl_3$. The interaction of the geometrically and electronically complementary units of C_{60} and exTTF by means of $\pi-\pi$ stacking, solvophobic, and concave–convex interactions has been confirmed by the slight shift—all resonances shift upfield, except those corresponding to the 1,3-dithiole rings that move downfield—and broadening of most resonances with increasing concentration (Figures 3 and S5, Supporting Information).[3d,f,27,28] A detailed analysis of these experiments demonstrates that only those resonances corresponding to the exTTF unit and to the fulleropyrrolidine ring shift with increasing concentration, leaving the signals of the oligomeric bridge practically unaltered. These findings suggest that the self-association of the conjugates is produced by the interaction of the geometrically and redox-active complementary units of exTTF and C_{60}, with the bridge being a mere spectator in the self-assembly process.

Variable-temperature ^{1}H NMR studies carried out for compounds **13** and **16** (Figures 4 and S7, Supporting Information) show features similar to those observed in the concentration dependence ^{1}H NMR experiments and confirm the self-association process of all these new conjugates. In addition, these ^{1}H NMR experiments demonstrate the inversion of the spatial arrangement of the nitrogen present in the fulleropyrrolidine ring.[29] The ^{1}H NMR spectrum of compound **16** at room temperature only presents one set of resonances for the geminal protons of the pyrrolidine ring ($\delta \approx 5.1$ and 4.1), which implies a fast exchange between the two extreme *cis* and *trans* conformations for this nitrogen atom regarding the organic addend. Decreasing the temperature below 258 K induces the apparition of two sets of well-defined resonances at $\delta \approx 5.1$. Below this temperature, the inversion barrier of the tertiary nitrogen is frozen and two formal chiral centers, namely, the nitrogen atom of the pyrrolidine ring and the carbon atom supporting the organic addend, appear to generate the two possible enantiomeric pairs in different proportions. A similar effect is also observed for the resonance at $\delta \approx 4.1$, rendering this process more energetic since only the broadening of the signal but not the appearance of two sets of resonances is observed in the range of temperatures studied (Figures 4 and S6, Supporting Information).

(23) We and others have experimentally observed that the oxidation processes of π-conjugated oligomers sometimes appear as broad and difficultly assignable waves in cyclic voltammetry. For recent examples, see: (a) Fernández, G.; Sánchez, L.; Veldman, D.; Wienk, M. M.; Atienza, C.; Guldi, D. M.; Janssen, R. A. J.; Martín, N. *J. Org. Chem.* **2008**, *73*, 3189–3196. (b) Zen, A.; Bilge, A.; Galbrecht, F.; Alle, R.; Meerholz, K.; Grenzer, J.; Neher, D.; Scherf, U.; Farrell, T. *J. Am. Chem. Soc.* **2006**, *128*, 3914–3915. (c) Narutaki, M.; Takimiya, K.; Otsubo, T.; Harima, Y.; Zhang, H.; Araki, Y.; Ito, O. *J. Org. Chem.* **2006**, *71*, 1761–1768. (d) Zhao, Y.; Shirai, Y.; Slepkov, A. D.; Cheng, L.; Alemany, L. B.; Sasaki, T.; Hegmann, F. A.; Tour, J. M. *Chem.—Eur. J.* **2005**, *11*, 3643–3658.

(24) A subsequent MALDI-TOF analysis carried out for the *para*-conjugated congener of dyad **5**, compound **9a** in ref 6c, has also allowed the observation of this unexpected behavior.

(25) The ability of a pristine exTTF molecule to recognize [60]fullerene or its derivative PCBM has been proven to be negligible: Otero, R.; Écija, D.; Fernández, G.; Gallego, J. M.; Sánchez, L.; Martín, N.; Miranda, R. *Nano Lett.* **2007**, *7*, 2602–2607.

(26) The travel time in MALDI-TOF experiments is directly proportional to the *m*/*z* value. Therefore, the ions corresponding to the aggregates formed from **16** need a longer time to reach the detector in comparison with the other conjugates, and they hold a higher possibility to disassemble. For a recent book on the utilization of the MALDI-TOF technique to detect supramolecular species, see: Schalley, C. *Analytical Methods in Supramolecular Chemistry*; Wiley: New York, 2007.

(27) (a) Pérez, E. M.; Capodilupo, A. L.; Fernández, G.; Sánchez, L.; Viruela, P. M.; Viruela, R.; Ortí, E.; Bietti, M.; Martín, N. *Chem. Commun.* **2008**, 4567–4569.

(28) The association constants (K_a) for compounds **5**, **10**, **13**, and **16** determined from these CD ^{1}H NMR investigations have been calculated in the range of 16–34 M^{-1}.

(29) Lukoyanova, O.; Kitaygorodskiy, A.; Cardona, C. M.; Echegoyen, L. *Chem.—Eur. J.* **2007**, *13*, 8294–8301.

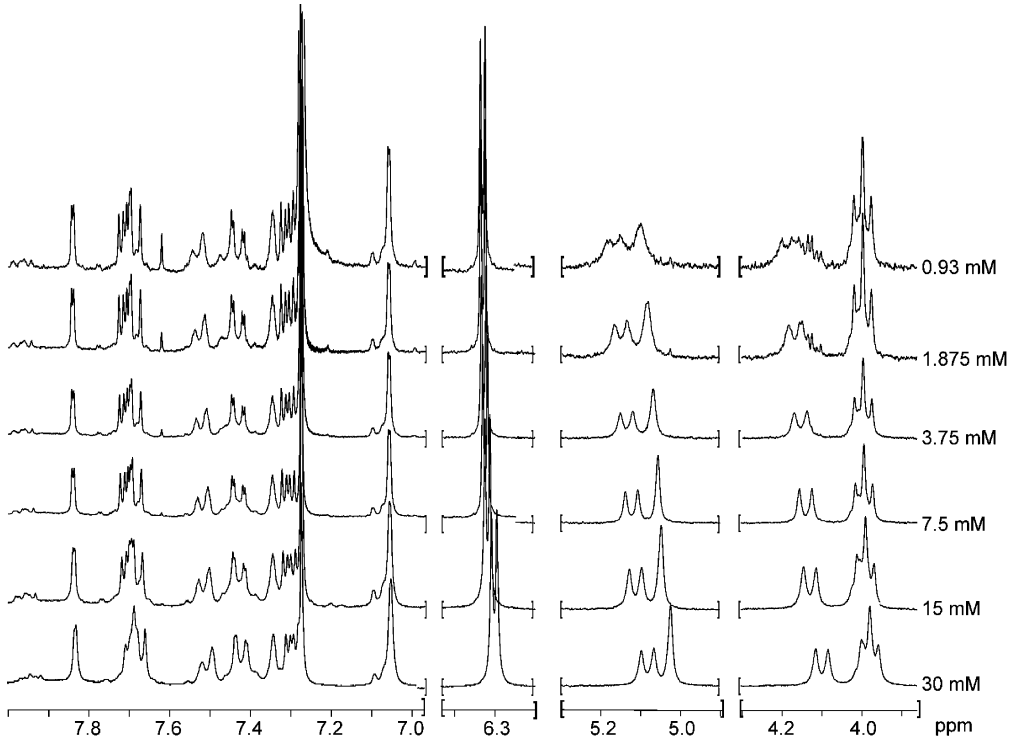

Figure 3. Partial ^{1}H NMR spectra ($CDCl_3$, 300 MHz, 298 K) of **10** at different concentrations.

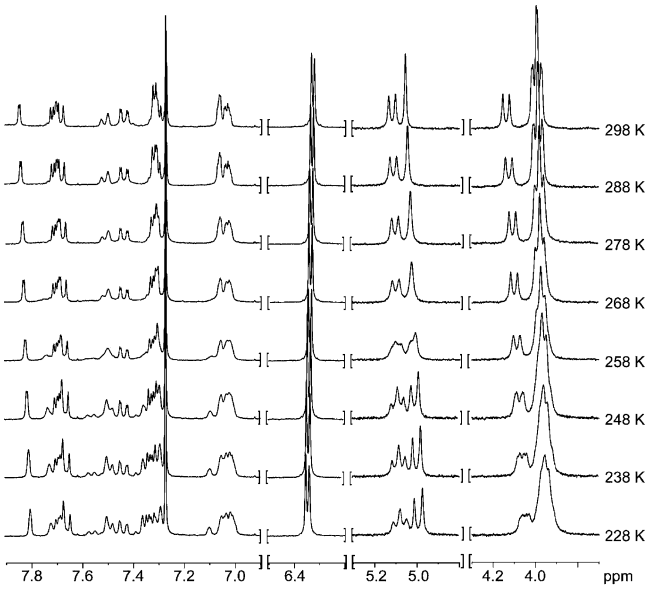

Figure 4. Partial variable-temperature ^{1}H NMR spectra (298−228 K, 4 mM, $CDCl_3$, 300 MHz) of **16**.

The self-assembly of **5**, **10**, **13**, and **16** onto solid supports was followed by atomic force microscopy (AFM) on mica. Figures 5 and S7 (Supporting Information) depict the AFM images obtained upon drop-casting $\sim 10^{-7}$ M solutions of **5**, **10**, **13**, and **16**. In all cases, reticulated networks are visible. These are of variable height and are constituted by interactive necklace-like wires. Isolated, individual wires are also observed, as demonstrated in Figure 5b,c. Height profiles that give rise to approximately 1 nm imply the presence of only one molecular unit.

Photophysical Properties. Photophysical means provide further insights into the organization of **5**, **10**, **13**, and **16**. For

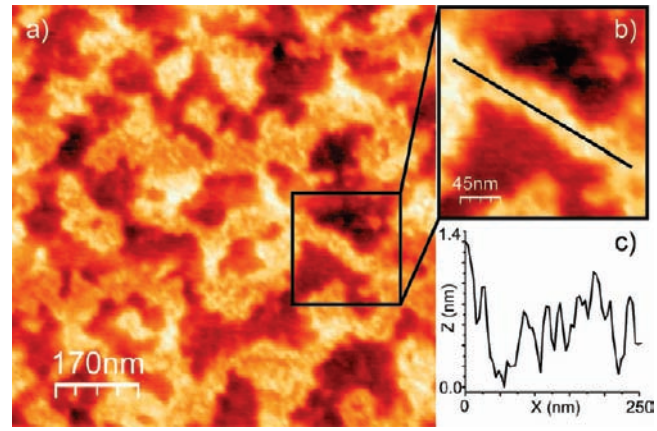

Figure 5. AFM images (tapping mode, air, 298 K) of a drop-cast chloroform solution of **13**: (a) large AFM image, (b) expanded area. (c) Height profile along the black line in (b).

optical measurements an asset of *meta*-linked phenyleneethynylene systems is their lack of conjugation, which keeps the visible range of the spectrum transparent—in contrast to the previously studied *para*-linked analogues, where the conjugation leads to a broad and intense absorption in the range of interest. In other words, for the *meta*-linked phenyleneethynylene systems the only significant contributions come from the absorptions of C_{60} (i.e., 434 and 705 nm) and exTTF (i.e., 450 nm). This opened the opportunity to test a wide range of concentrations and follow the developments of intracomplex hybrids by spectroscopic means.[30] For example, with increasing concentrations, we note that in toluene a distinct new absorption develops—red-shifted relative to that of exTTF—at 470 nm.

(30) (a) Giacalone, F.; Segura, J. L.; Martín, N.; Guldi, D. M. *J. Am. Chem. Soc.* **2004**, *126*, 5340–5341. (b) de la Torre, G.; Giacalone, F.; Segura, J. L.; Martín, N.; Guldi, D. M. *Chem. Eur. J.* **2005**, *11*, 1267–1280.

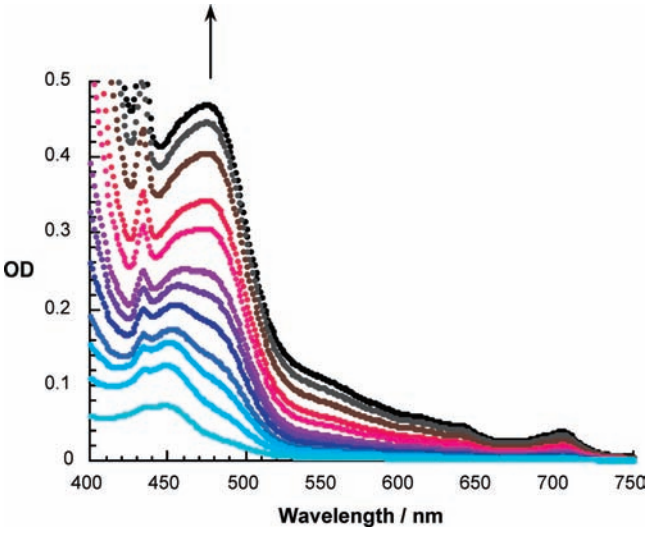

Figure 6. Absorption spectra of a toluene solution of **10** with increasing concentrations (5.5×10^{-6}, 9.3×10^{-6}, 1.2×10^{-5}, 1.3×10^{-5}, 1.6×10^{-5}, 1.8×10^{-5}, 2.0×10^{-5}, 2.4×10^{-5}, 2.8×10^{-5}, 3.4×10^{-5}, 3.9×10^{-5}, and 4.3×10^{-5} M). Arrows indicate the progression of the titration and the development of the new features.

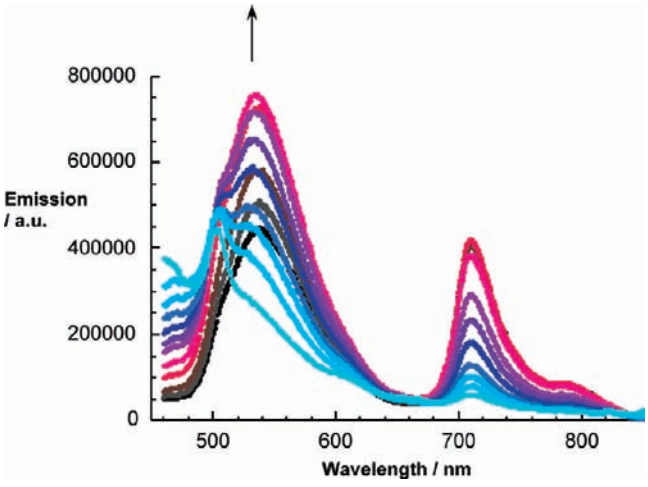

Figure 7. Emission spectra of a toluene solution of **10** with increasing concentrations (5.5×10^{-6}, 9.3×10^{-6}, 1.2×10^{-5}, 1.3×10^{-5}, 1.6×10^{-5}, 1.8×10^{-5}, 2.0×10^{-5}, 2.4×10^{-5}, 2.8×10^{-5}, 3.4×10^{-5}, 3.9×10^{-5}, and 4.3×10^{-5} M). Arrows indicate the progression of the titration and the development of the new features.

Throughout these concentration variations the C_{60} and exTTF features remain visible; see Figure 6. In oDCB and benzonitrile the absorptions shift to 485 and 495 nm, respectively. Interestingly, these changes are only discernible for **10**, **13**, and **16**. In **5**, on the other hand, intramolecular C_{60}−exTTF interactions dominate over intermolecular C_{60}−exTTF interactions and, in turn, hamper in the concentration of the photophysical experiments the formation of intracomplex hybrids. Steric hindrance might also contribute to the suppression of the self-organization.

When turning to complementary emission experiments, we note several changes. First, in the blue region the broad and structureless exTTF emission transforms—only for **10**, **13**, and **16**—with increasing concentration into a new band (Figure 7). The latter is essentially a mirror image of what has been seen in the absorption measurements. In toluene the emission band maximizes at 533 nm, which again shifts to the red when more polar solvents are used: 550 nm in *o*-dichlorobenzene and 575 nm in benzonitrile. Moreover, a complementary excitation spectrum confirms the origin of the new emission band (Figure 8). We interpret this new band as being due to charge transfer interactions. These take the form of a shift of electron density from exTTF to C_{60} to give a polar state that is solvated better in the more polar solvents. Inspecting **10**, **13**, and **16**, a distinct stabilization of the interactions is reflected by a continuous red shift from 533 nm (**10**) to 537 nm (**13**) and 554 nm (**16**); all values are cited for toluene. Typical quantum yields of these emissive features, which depend on the structure and the solvent are on the order of 10^{-3}.[31] In particular, they tend to be lower in polar media than in nonpolar media—a trend that is well understood on the basis of excited-state relaxations. For example, **10** gives rise to emission maxima at 533, 550, and 575 nm in toluene, *o*-dichlorobenzene, and benzonitrile, respectively. Notable is the correlation with the corresponding absorption maxima at 470, 485, and 495 nm. Similar conclusions were previously derived for C_{60}−exTTF[13] and C_{60}−ZnP[31] charge transfer absorption and emission features. Second, in the red region we note the C_{60}-centered emission with a maximum around 710 nm. The position of the maximum lacks any susceptibility with respect to the solvent polarity. Nevertheless, it is quenched (i.e., $<3.0 \times 10^{-4}$) when compared to the C_{60} reference (i.e., 6.0×10^{-4}).[10]

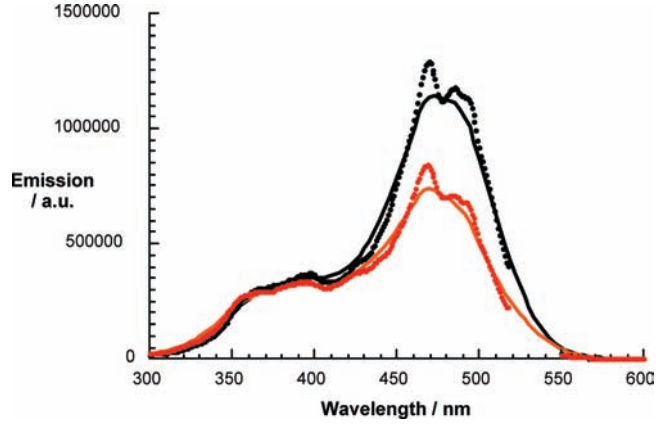

Figure 8. Excitation spectra of **10** (orange) and **13** (black) in toluene solution monitoring the emission at 530 nm.

For a 1:1 stoichiometry, the change in fluorescence intensity (ΔI) is related to the association constant (K) by a Benesi−Hildebrand-type equation:[32]

$$\Delta I/c = K\Delta I_{\infty} - K\Delta I$$

where ΔI_{∞} is the maximum change in fluorescence intensity when all molecules form the complex. Using this method we

(31) Guldi, D. M.; Scheloske, M.; Dietel, E.; Hirsch, A.; Troisi, A.; Zerbetto, F.; Prato, M. *Chem.—Eur. J.* **2003**, *9*, 4968–4979.

(32) The association constants (K) were determined for the explicit association between exTTF and C_{60} with a 1:1 complex stoichiometry. The complex formation is associated with a newly developing charge transfer absorption, whose equilibrium is expressed by the Benesi−Hildebrand method. To this end, we have used the concentration dependence to determine the association constant according to Benesi−Hildebrand: Benesi, H. A.; Hildebrand, J. H. *J. Am. Chem. Soc.* **1949**, *71*, 2703−2707. Assuming weak complexation constants (i.e., $K \approx 1000\ M^{-1}$) combined with appreciable absorption changes, this method provides reasonable results: Yang, C.; Liu, L.; Mu, T.-W.; Guo, Q.-X. *Anal. Sci.* **2000**, *16*, 537–540. In turn, it has emerged as a versatile tool for describing the 1:1 association of organic charge transfer complexes. *Organic Charge-Transfer Complexes*; Foster, R., Ed.; Academic Press: London, 1969; p 125.

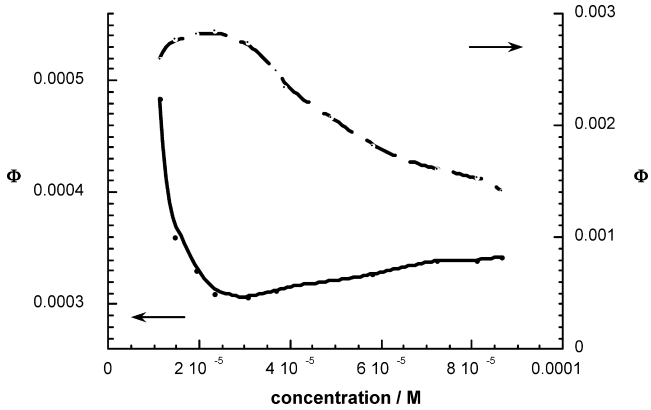

Figure 9. Charge transfer emission (dashed line, right *x*-axis) versus C_{60} emission (solid line, left *x*-axis) quantum yields of an *o*DCB solution of **10**.

have calculated the binding constants (K) as 1.1×10^3 M^{-1} (**10**), 2.1×10^3 M^{-1} (**13**), and 1.4×10^3 M^{-1} (**16**). Since no appreciable charge transfer fluorescence was observed for **5**, the evaluation of an association constant was dispensable.

In the low concentration regime (10^{-6} M), where the electron donor−acceptor conjugates are present in their monomeric form, the fluorescence quenching is likely due to intramolecular processes. An electron transfer deactivation that takes place between the electron-donating exTTF and the electron-accepting C_{60} leads to the formation of a radical ion pair state—vide infra.[14] Notable is in this context that running a solvent dependence (i.e., toluene, *o*-dichlorobenzene, benzonitrile) on the fluorescence quenching reveals changes only for **5** (i.e., toluene, 1.2×10^{-4}; *o*-dichlorobenzene, 7.6×10^{-5}; benzonitrile, 2.2×10^{-5}). All others, that is, **10** ($(1.0 \pm 0.3) \times 10^{-4}$), **13** ($(1.2 \pm 0.3) \times 10^{-4}$), and **16** ($(1.8 \pm 0.3) \times 10^{-4}$), give rise to nearly invariable quantum yields regardless of the solvent. This indicates for **10**, **13**, and **16** distinct through space interactions, while through bond interactions are likely to exist in **5**. Similar conclusions, that is, through space interactions, were noted for flexibly linked C_{60}−donor systems.[33] Implementation of a flexible linker is thought to enable intramolecular rearrangements that are driven by charge transfer interactions. In other words, C_{60}−donor systems adapt a folded—with close C_{60}−donor proximities—rather than a stretched conformation.[34] An increase in the overall concentration (up to 10^{-4} M) evokes a further decrease of the C_{60} fluorescence quantum yields. Since these experiments are always set in relation to the C_{60} reference, we propose that now an alternative electron transfer deactivation dominates the photoreactivity of C_{60} and exTTF. Implicit is a scenario which involves tied charge transfer interactions between C_{60} and exTTF, that is, intracomplex processes in the newly formed intracomplex hybrids. Interestingly, both emission features track each other; the charge transfer emission band reaches its maximum at a concentration where the C_{60} fluorescence quenching is at its peak (Figure 9).

Time-resolved fluorescence measurements could not provide further details about the competition between intramolecular and intracomplex processes. In fact, we only see a component that we ascribe to the intramolecular process with a rate constant of 1.5×10^9 s^{-1}. We believe, however, that only the lack of time resolution is responsible for this ambiguous trend.

The aforementioned trends indicated the need for further investigations, namely, testing the C_{60}−exTTF systems by transient absorption measurements. In particular, excitations at 387 and 482 nm were chosen to photoexcite the ground state of C_{60}, exTTF, and the C_{60}−exTTF monomer and the charge transfer state of the intracomplex hybrids, respectively.

Photoexcitation of exTTF at 387 nm generates an exTTF-centered excited state. Spectral characteristics of this very short-lived excited state (1.2 ps) are transient maxima around 465, 605, and 990 nm as well as transient bleaching at <450 nm. The short lifetimes (i.e., after 5 ps no transient absorption remains) are rationalized by the presence of the sulfur atoms, with a strong second-order vibronic spin−orbit coupling. Going beyond our femtosecond experiments (i.e., 3 ns) we tested exTTF in nanosecond experiments following 355 nm excitation. However, outside of the 10 ns time window of the instrumental time resolution, no notable transients were detected.

The singlet excited state of C_{60}, on the other hand, displays a distinctive singlet−singlet transition around 880 nm.[35] The latter undergoes a quantitative but nevertheless slow (i.e., 5×10^8 s^{-1}) intersystem crossing to yield the long-lived triplet manifold, for which maxima are noted at 360 and 700 nm, followed by a low-energy shoulder at 800 nm.

Now, when turning to the C_{60}−exTTF systems, photoexcitation at 387 nm in the low concentration regime should be discussed first. Detecting the instantaneous grow-in of the 880 nm absorption affirms the successful C_{60} excitation—similar to what has been seen for the reference experiments with C_{60}. Instead of seeing, however, the slow intersystem crossing dynamics, the singlet−singlet absorption decays in the presence of exTTF donors with accelerated dynamics. The singlet-excited-state lifetimes, as they were determined from an average of first-order fits of the time−absorption profiles at various wavelengths, are on the order of 30 ps. Spectroscopically, the transient absorption changes, taken after the completion of the decay, bear no resemblance to the C_{60} triplet excited state. In particular, the new transients reveal strong maxima in the visible range—at ~680 nm—which match those of the one-electron-oxidized exTTF radical cations, while in the near-infrared—at ~1000 nm—features evolve that are a close spectral match to those of the one-electron-reduced C_{60} radical anion (Figure 10).[36] In other words, our spectroscopy confirms the formation of intramolecular radical ion pair states—formed through bond in **5** and through space in **10**, **13**, and **16**. The latter are metastable on the femto/picosecond time scale. This required examining the charge-recombination dynamics on the nanosecond time scale. Therefore, the same solutions were excited with a 6 ns laser pulse. In this context, the spectral fingerprints of the radical ion pair state—as seen immediately after the nanosecond laser pulse—are useful probes (Figure 11). Important is the fact that

(33) (a) Guldi, D. M. *Pure Appl. Chem.* **2003**, *75*, 1069–1076. (b) Guldi, D. M. *Chem. Soc. Rev.* **2002**, *31*, 22–36. Herranz, M. A.; Ehli, C.; Campidelli, S.; Gutiérrez, M.; Hug, G. L.; Ohkubo, K.; Fukuzumi, S.; Prato, M.; Martín, N.; Guldi, D. M. *J. Am. Chem. Soc.,* **2008**, *130*, 66–73.

(34) Schuster, D. I.; MacMahon, S.; Guldi, D. M.; Echegoyen, L.; Braslavsky, S. E. *Tetrahedron* **2006**, *62*, 1928–1936. (a) Guldi, D. M.; Hungerbühler, H.; Asmus, K.-D. *J. Phys. Chem.* **1995**, *99*, 9380–9385. (b) Guldi, D. M.; Sánchez, L.; Martín, N. *J. Phys. Chem. B* **2001**, *105*, 7139–7144.

(35) (a) Becke, A. D. *J. Chem. Phys.* **1993**, *98*, 5648–5653. (b) Burke, K.; Perdew, J. P.; Wang, Y. In *Electronic Density Functional Theory: Recent Progress and New Directions*; Dobson, J. F., Vignale, G., Das, M. P., Eds.; Plenum: New York, 1998.

(36) (a) Ditchfield, R.; Hehre, W. J.; Pople, J. A. *J. Chem. Phys.* **1971**, *54*, 724–728. (b) Rassolov, V. A.; Pople, J. A.; Ratner, M. A.; Windus, T. L. *J. Chem. Phys.* **1998**, *109*, 1223–1226.

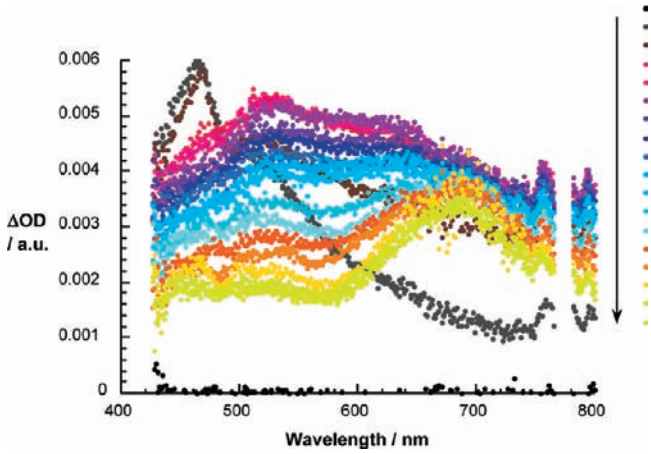

Figure 10. Differential absorption spectra (visible) obtained upon femtosecond flash photolysis (387 nm) of **10** (10^{-6} M) in nitrogen-saturated *o*-dichlorobenzene solutions with time delays between 0 and 3000 ps at room temperature (black, 0 ps; gray, 1 ps; yellow, 2900 ps).

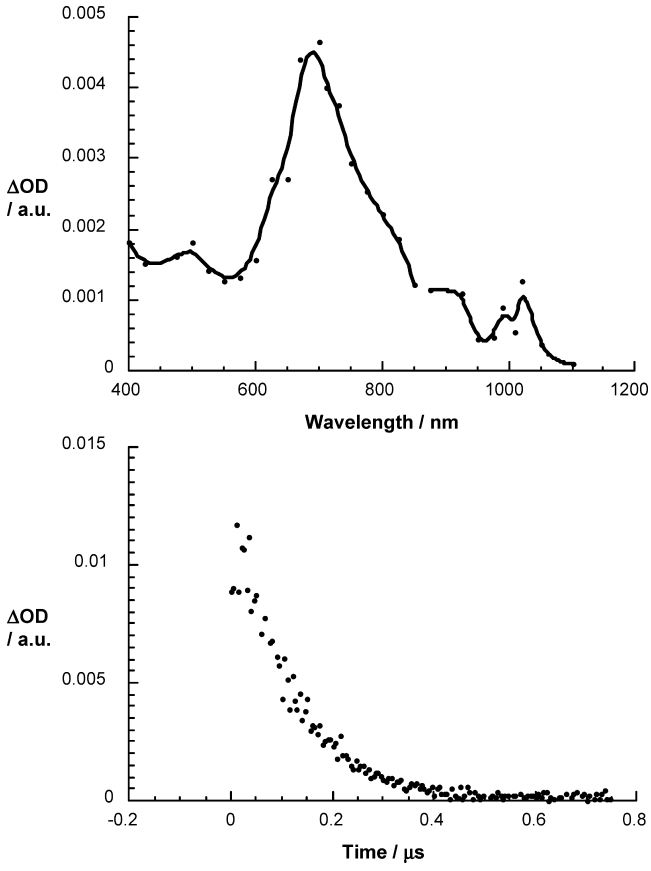

Figure 11. (a) Differential absorption spectrum (visible and near-infrared) obtained upon nanosecond flash photolysis (355 nm) of **10** (2.0×10^{-6} M) in nitrogen-saturated *o*-dichlorobenzene solutions with a time delay of 100 ns at room temperature, indicating the radical ion pair state features at 680 and 1010 nm. (b) Time−absorption profile of the spectrum shown above at 675 nm to monitor the decay of the radical ion pair state.

the decays of both probes resemble each other and give rise to kinetics that obey a clean unimolecular rate law. The lifetimes are on the order of tens of nanoseconds for **10** (i.e., 26 ns), **13** (i.e., 41 ns), and **16** (i.e., 49 ns), where the reactivity is driven by through space interactions. Different is the scenario for **5**,

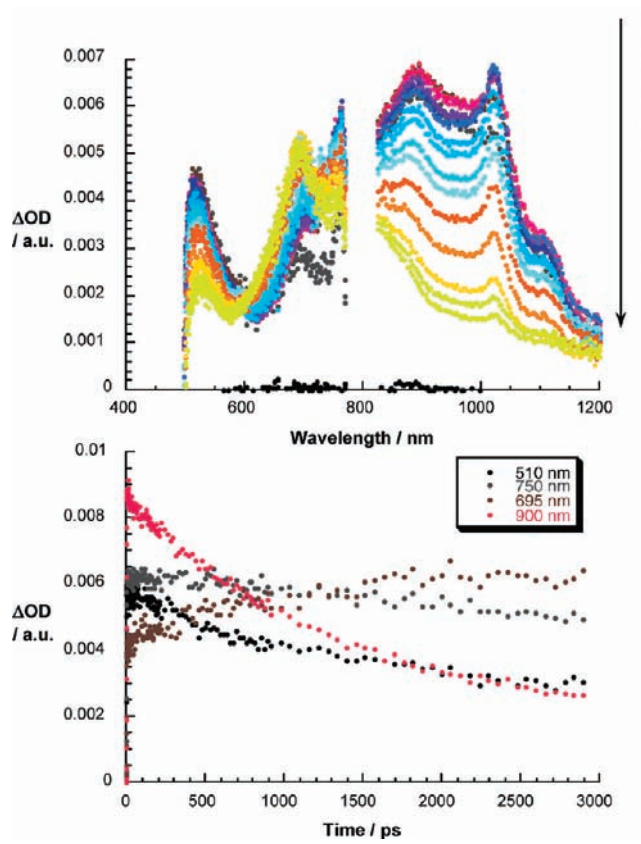

Figure 12. (a) Differential absorption spectra (visible and near-infrared) obtained upon femtosecond flash photolysis (482 nm − 150 nJ) of **10** (2.0×10^{-4} M) in nitrogen-saturated *o*-dichlorobenzene solutions with time delays between 0 and 3000 ps at room temperature (black, 0 ps; blue, 10 ps; yellow, 2900 ps). (b) Time−absorption profiles of the spectra shown above at 510, 695, 750, and 900 nm to monitor the formation of the radical ion pair state.

where through bond interactions lead to lifetimes of 128 ns again, at low concentrations (Figures S8, Supporting Information).

In stark contrast, excitation into the charge transfer bands, that is, in the high concentration regime, evokes the immediate formation of the radical ion pair state; see Figure 12. In particular, the exTTF radical cation and the C_{60} radical anion features evolve nearly instantaneously (∼1 ps) at 680 and 1000 nm, respectively.[13] This confirms the rapid formation of the intracomplex radical ion pair state. The lifetime of this intracomplex radical ion pair state is remarkably long, exceeding the time scale of our femtosecond experiments. It is on the nanosecond time scale, where the same radical ion pair features are generated, which allows determining the lifetimes as 4.0 ± 0.7 μs (**10**, 3.2 μs; **13**, 4.7 μs; **16**, 4.6 μs); an example is illustrated in Figure 13. Such lifetimes infer a significant stabilization relative to the monomer forms at low concentrations. An intracomplex hopping mechanism is likely to be responsible for longer lifetimes, since larger charge separation distances are realized.

Modeling. Density functional theory (DFT) and semiempirical molecular orbital (MO) theory were used to characterize the charge transfer features of the donor−bridge−acceptor conjugates. Because of the high computational demands of systems of the size of those considered here, only monomeric **5**, **10**, **13**, and **16** were investigated. Geometry optimizations at the B3PW91[35]/6-31G**[36] DFT[37] level gave almost coplanar

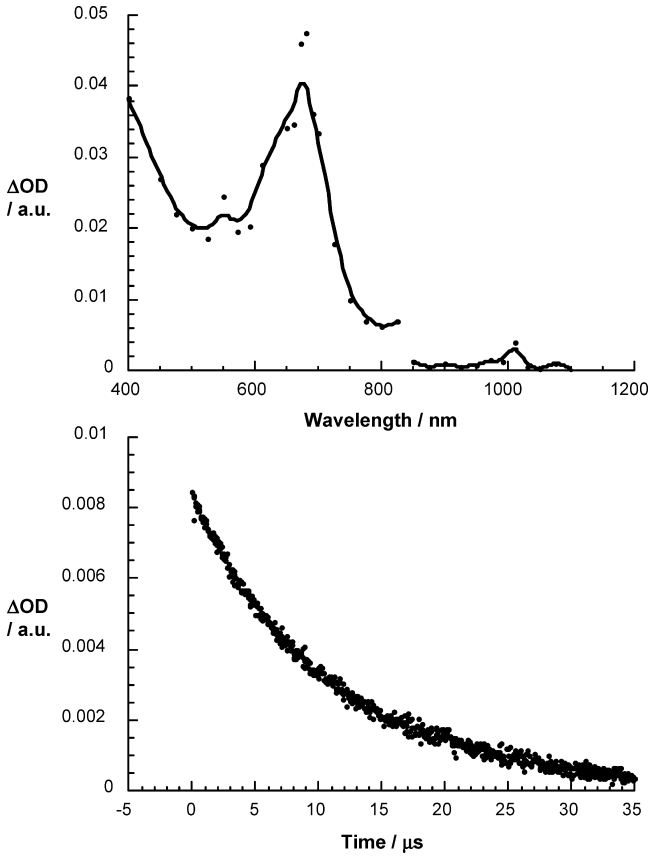

Figure 13. (a) Differential absorption spectrum (visible and near-infrared) obtained upon nanosecond flash photolysis (355 nm) of **10** (2.0×10^{-4} M) in nitrogen-saturated *o*-dichlorobenzene solutions with a time delay of 100 ns, indicating the radical ion pair state features at 680 and 1010 nm. (b) Time−absorption profile of the spectrum shown above at 650 nm to monitor the decay of the radical ion pair state.

conformations of the bridge for all isomers. Coplanarity of the phenyl rings in oligo(phenyleneethynylene)s (OPEs) is favored by π-overlap, but the calculations also reveal very low rotation barriers. Nevertheless, the *meta* connectivity weakens the π-conjugation in comparison to the strongly conjugated oligo(*p*-phenyleneethynylene)s (OPPEs), as also suggested by the absorption spectra, which reveal only absorption features due to C_{60} and exTTF.

Analysis of the frontier orbital schemes (Figure 14) corroborates that the highest occupied orbitals are localized on the electron-donating exTTF, whereas the lowest unoccupied orbitals are localized on C_{60}. Important is that the bridge orbitals are energetically well separated from the frontier orbitals, resulting in virtually no overlap between the electron donor, the bridge, and the electron acceptor. In line with this picture, the HOMO − 1 to LUMO + 2 orbitals of all C_{60}−exTTF systems reveal almost equal orbital energies independently of the length of the bridge (Table S1, Supporting Information).

Not only the ground-state features but also those of the excited states are relevant for interpreting the photophysical experiments. In this context, we have used semiempirical configuration interaction (CI) calculations with the AM1* [38] Hamiltonian, which includes d-orbitals on sulfur. First singles-only CI (CIS) calculations with varying numbers of active orbitals were used to judge the size of the CI window necessary to achieve convergence of the results. An active window of 15 occupied and 15 virtual orbitals gave a full description of the electronic states of the C_{60}−exTTF systems. In the current context, we

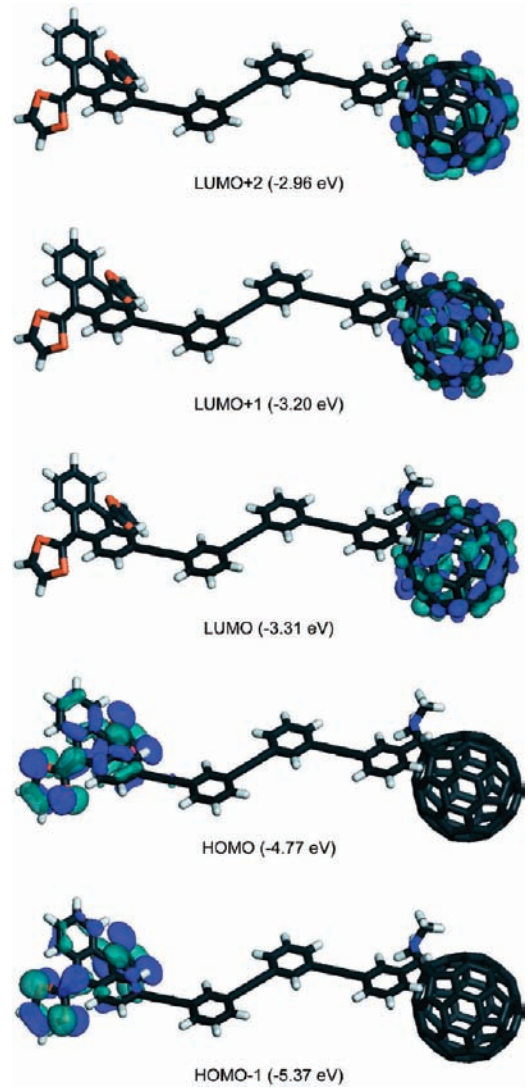

Figure 14. Representative frontier orbital schemes of **13** given by DFT calculations including the orbital energies.

will address only the locally excited and the charge transfer states of the monomers. In all systems the locally excited states are attributed to electronic excitations of exTTF with oscillator strengths on the order of $f \approx 0.5$. The singlet-excited-state energies calculated in vacuo (3.2 eV) are consistent with those found throughout the absorption studies. In all C_{60}−exTTF systems, two distinct charge transfer states emerge that are dominated by the HOMO → LUMO and HOMO → LUMO + 1 excitations. The orbital scheme shown in Figure 14 implies that these states correspond to a charge transfer from exTTF (HOMO) to C_{60} (LUMO/LUMO + 1). The change in the dipole moment on excitation (μ) confirms the charge transfer nature of these excited states. In particular, μ values that range between 43 and 157 D (Table S2, Supporting Information) are due to charge-separated excited states. To evaluate any bridge effects,

(37) All DFT calculations were performed using the Gaussian 03 program package: Frisch, M. J.; et al. *Gaussian 03*, revision D.02; Gaussian, Inc.: Wallingford, CT, 2004.
(38) Winget, P.; Horn, A. H. C.; Selcuki, C.; Martin, B.; Clark, T. *J. Mol. Model.* **2003**, *9*, 408–414.
(39) Rauhut, G.; Clark, T.; Steinke, T. *J. Am. Chem. Soc.* **1993**, *115*, 9174–9181.

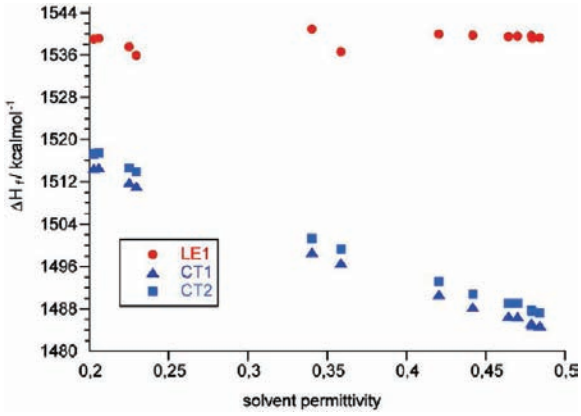

Figure 15. Dependence of the calculated heats of formation, ΔH_f, on the solvent permittivity (i.e., $(\varepsilon - 1)/(2\varepsilon + 1)$, for the discussed states of **16** as a representative example: locally excited state (red circles), CT state 1 (blue triangles), CT state 2 (blue squares).

we have added the directly linked donor−acceptor system (the 0-mer; see Figure S9, Supporting Information) to our CI calculations.

For **5** and the 0-mer, two charge transfer states were computed at excitations between 372 and 381 nm (3.2−3.3 eV), which are a perfect match to the experimental results. In both of these C_{60}−exTTF systems, these transitions are accompanied by a change of dipole moment (i.e., μ) that is on the order of 45 D. In **10**, **13**, and **16**, the charge transfer transitions go along with much larger changes in the dipole moment, reaching 97 D for **10**, 125 D for **13**, and 155 D for **16**. These very large dipole moments and the very low (essentially zero) oscillator strengths confirm the charge transfer nature of the transitions and help confirm the radical ion pair formation as found by time-resolved absorption spectroscopy in the low-concentration regime (vide supra). Furthermore, the dipole changes are consistent with those previously published for the corresponding *para*-conjugated systems (OPPEs).[15a] They correspond to charge separations (+1 and −1 electronic charges) of 20, 26, and 32 Å for **10**, **13**, and **16**, respectively. The maximum possible distances (i.e., those in the fully extended conformations shown in Scheme 2) between the centers of C_{60} and the exTTF moiety in these three compounds are approximately 22, 28, and 35 Å, respectively. Obviously, the interplay between C_{60} and exTTF is in **5**/0-mer augmented by short bridge lengths favoring through bond charge transfer interactions/enhanced electronic coupling. This, in turn, lowers the activation barriers for charge separation processes in **5**. In addition, the close proximity of the donor and acceptor moieties in **5** results in a low dipole moment in the charge-separated state. On the other hand, the energy penalties that are applicable in **10**, **13**, and **16** point to the necessities of through space interactions/solvent stabilization, which become increasingly important as the distances between the donor and acceptor increase from **10** to **16**.

Finally, we have investigated solvent effects using the self-consistent reaction field (SCRF) within the polarizable continuum model (PCM).[39] Here, solvent stabilizations of the charge transfer states are directly implemented. In comparison to the calculations performed in vacuo, solvent effects assist in lowering the energies of the charge transfer states relative to those of the locally excited states. This implies energetic stabilization of the charge-separated species in polar media (Figure 15). Notably, enhanced solvent stabilizations were indeed found for **10**, **13**, and **16**. This proves the favorable

Scheme 3. Energy Diagram Showing the Excited-State Deactivation Pathways in C_{60}−exTTF at Low Concentrations (**5**, **10**, **13**, and **16**) and at High Concentrations (**10**, **13**, and **16**)

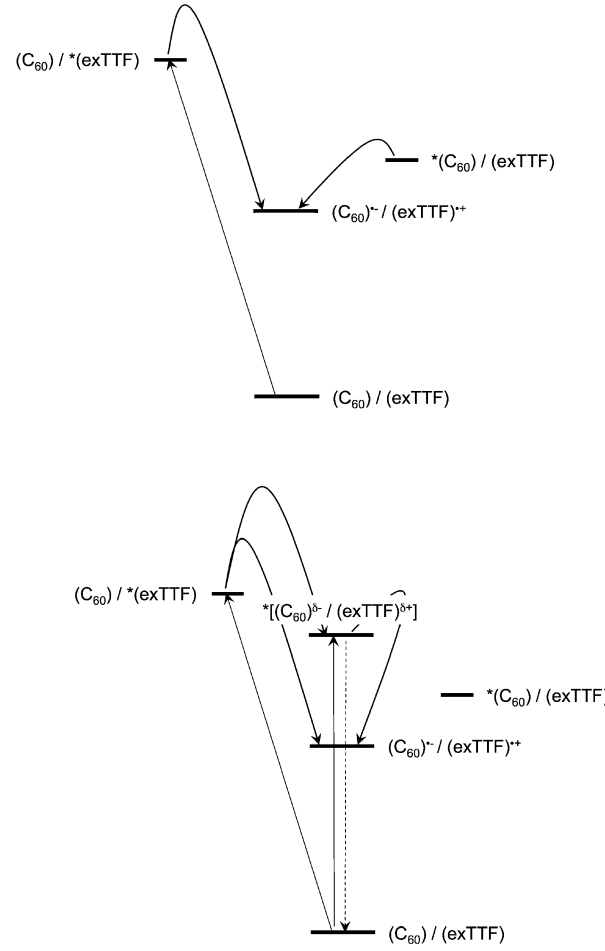

charge transfer features in **5**, for which already calculations in vacuo revealed energetically lower charge transfer states in comparison to the locally excited state (Table S2, Supporting Information). Note that one might instinctively expect even stronger solvent stabilization of the CT state, which has a dipole moment of 155 D for **16**. The increase in solvation energy of approximately 30 kcal mol^{-1} on increasing the solvent permittivity from 0.2 to 0.5 is, however, consistent with the calculated dipole moment of the excited state. The standard Kirkwood−Onsager expression for the free energy gives an effective spherical cavity radius for the proposed CT state of 22 Å for **16** assuming that the dipole moment is 155 D. This value is reasonable for **16**, for which we estimate that the centers of charge are approximately 35 Å apart. We emphasize, however, that the SCRF model used for the calculations is far more sophisticated than the Onsager model and that the estimate provided above only serves to underline the reliability of both the assignment of the CT state and the solvation calculations.

Conclusions

In summary, a series of new electron donor−acceptor conjugates (**5**, **10**, **13**, and **16**) have been synthesized, and different techniques (MALDI-TOF, CD ^{1}H NMR, and fluorescence and AFM imaging) demonstrate their self-organization in the gas phase, in solution, and on solid substrates and test them in electron transfer reactions. Important is the motif that powers and controls the self-organization, namely, combining

convex C_{60}—as an electron acceptor—and concave exTTF—as an electron donor—that are bridged by *m*-phenyleneethynylene spacers. A unique asset is that the choice of *m*-phenyleneethynylene assists in tuning the charge transfer features (i.e., charge separation and charge recombination). In particular, implementing just one *m*-phenyleneethynylene ring (**5**) leads to intramolecular electron transfer that is exclusively and independent of the concentration (10^{-6} to 10^{-4} M) driven by a "through bond" mechanism. This is rationalized on grounds of steric hindrance, which suppresses the self-organization. Different is the picture when using two, three, or even four *m*-phenyleneethynylene rings. At low concentration (10^{-6} M) "through space" intramolecular electron transfer events are favored; see Scheme 3. Here, both excited states, that is, exTTF (2.75 eV) and C_{60} (1.78 eV), decay via the transient intramolecular radical ion pair state (1.2 eV). These interactions are, however, quite ineffective and, in turn, lead to excited-state deactivations that are at high concentrations (10^{-4} M) dominated by intracomplex charge transfer events, namely, between exTTF of one molecule and C_{60} of another molecule that are self-organized into wormlike structures. In fact, distinct charge transfer features (i.e., absorption and emission) evolve. The charge transfer emissions imply—besides large electronic coupling matrix elements—slow radiative decays and small reorganization energies. In fact, the inner ($\lambda_V = (\lambda_{absorption} + \lambda_{emission})/2$) and outer ($\lambda_S = -\lambda_{emission} - \Delta G_{CR}$) reorganization energies were derived with the help of the charge transfer absorption ($\lambda_{absorption}$) and emission ($\lambda_{emission}$) maxima. In **10**, for example, the total reorganization energies range from 0.5 eV (toluene) to 0.83 eV (benzonitrile). Notable is the contribution of exTTF, whose substantial structural reorganization evokes a rather large reorganization energy. In the corresponding C_{60}−ZnP charge transfer systems, the lack of structural changes upon ZnP oxidation leads to smaller values. The distinct charge transfer states in **10**, **13**, and **16** (2.47 eV in toluene, 2.40 eV in *o*-dichlorobenzene, 2.32 eV in benzonitrile) convert upon photoexcitation into fully $C_{60}^{\bullet-}$−$exTTF^{\bullet+}$ charge-separated states (1.2 eV in *o*-dichlorobenzene); see Scheme 3. Implicit is that, among the localized singlet excited states, only the singlet excited state of exTTF (2.75 eV) is able to deactivate via the charge transfer state, while that of C_{60} (1.78 eV) is energetically insufficient to populate the latter.

At higher concentration (10^{-4} M) through space intramolecular electron transfer events are quite ineffective and, in turn, lead to excited-state deactivations that are dominated by intracomplex electron transfer events, namely, between exTTF of one molecule and C_{60} of another molecule that are self-organized into wormlike structures. Additionally, the self-organization assists in stabilizing the resulting radical ion pair state with lifetimes up to 4.7 μs. Such values reflect a remarkable stabilization of more than 2 orders of magnitude—3.2−4.7 μs versus 26−49 ns.

Acknowledgment. Financial support was provided by the MEC of Spain (Projects CTQ2008-00795/BQU and Consolider-Ingenio 2010C-07-25200), CAM (MADRISOLAR Project P-PPQ-000225-0505), UCM (Grant UCM-SCH-PR34/07-15826), Deutsche Forschungsgemeinschaft (Grant SFB 583), and Office of Basic Energy Sciences of the United States. A.M.-O., G.F., and A.G. thank the CAM and MEC of Spain for a research grant and a Ramón y Cajal contract, respectively. We are thankful to A. Soubrié (Centro de Microscopía y Citometría, UCM) for AFM imaging and Dr. M. Alonso (UAM) for the MALDI-TOF spectra. We thank Dr. J. L. Delgado for his help in the synthetic protocols.

Supporting Information Available: Experimental procedures with complete spectroscopic and structural analysis, including Figures S1−S10. This material is available free of charge via the Internet at http://pubs.acs.org.

JA9024269